Available online at www.sciencedirect.com
SCIENCE DIRECT®
Journal of Crystal Growth 277 (2005) 578–592
JOURNAL OF CRYSTAL GROWTH
www.elsevier.com/locate/jcrysgro

Nonlinear stability analysis of self-similar crystal growth: control of the Mullins–Sekerka instability

Shuwang Li[a,b], John S. Lowengrub[b,*], Perry H. Leo[a], Vittorio Cristini[b,c]

[a]*Department of Aerospace Engineering and Mechanics, University of Minnesota, Minneapolis, MN 55455, USA*
[b]*Department of Mathematics, University of California at Irvine, 103 MSTB, Irvine, CA 92697, USA*
[c]*Department of Biomedical Engineering, University of California at Irvine, Irvine, CA 92697, USA*

Received 14 July 2004; accepted 16 December 2004
Communicated by G.B. McFadden
Available online 3 February 2005

Abstract

In this paper, we perform a stability analysis of 2D, noncircular self-similar crystals with isotropic surface tension growing in a supercooled melt. The existence of such self-similarly growing crystals was demonstrated recently in our previous work (J. Crystal Growth 267 (2004) 703). Here, we characterize the nonlinear morphological stability of the self-similar crystals, using a new spectrally accurate 2D boundary integral method in which a novel time and space rescaling is implemented (J. Crystal Growth 266 (2004) 552). This enables us to accurately simulate the long-time, nonlinear dynamics of evolving crystals. Our analysis and simulations reveal that self-similar shapes are stable to perturbations of the critical flux for self-similar growth. This suggests that in experiments, small oscillations in the critical flux will not change the main features of self-similar growth. Shape perturbations may either grow or decay. However, at long times there is nonlinear stabilization even though unstable growth may be significant at early times. Interestingly, this stabilization leads to the existence of universal limiting shapes. In particular, we find that the morphologies of the nonlinearly evolving crystals tend to limiting shapes that evolve self-similarly and depend on the flux. A number of limiting shapes exist for each flux (the number of possible shapes actually depends on the flux), but only one is universal in the sense that a crystal with an arbitrary initial shape will evolve to this universal shape. The universal shape can actually be retrograde. By performing a series of simulations, we construct a phase diagram that reveals the relationship between the applied flux and the achievable symmetries of the limiting shapes. Finally, we use the phase diagram to design a nonlinear protocol that might be used in a physical experiment to control the nonlinear

*Corresponding author. Tel.: +1 9498242655; fax: +1 9498247993.
E-mail addresses: sli@aem.umn.edu (S. Li), lowengrb@math.uci.edu (J.S. Lowengrub), phleo@aem.umn.edu (P.H. Leo), cristini@math.uci.edu (V. Cristini).

0022-0248/$ - see front matter
doi:10.1016/j.jcrysgro.2004.12.042

morphological evolution of a growing crystal. Because our analysis shows that interactions among the perturbation modes are similar in both 2D and 3D, our results apply qualitatively to 3D.

PACS: 81.10.A; 64.70.D

Keywords: A1. Compact growth; A1. Crystal growth; A1. Diffusion; A1. Morphological stability; A1. Mullins–Sekerka instability; A1. Self-similar

1. Introduction

The morphological stability of a growing crystal in the supercooled melt is a fundamental problem in phase transformations and has been extensively studied theoretically (e.g. Refs. [1–13,20–23]) and experimentally (e.g. Refs. [14–19]). Crystal growth is typically characterized by the formation of complex morphologies due to the Mullins–Sekerka instability. For example starting from a compact circular or spherical-like seed, cellular, dendritic growing shapes are widely observed during growth. In many applications (e.g. castings) it is desirable to suppress the instability and prevent the formation of dendrites. In this paper, we characterize the nonlinear morphological stability of a growing crystal through *long time* simulations by perturbing the noncircular, self-similar solutions we have found recently [3]. This stability analysis shows the existence of nonlinear limiting shapes resulting from the evolution, and identifies the protocols by which the compact growth of crystals with a desired symmetries can be achieved even in the nonlinear regime of growth.

It has long been recognized that growth morphologies are determined by the interaction between macroscopic driving forces (supercooling) and microscopic interfacial properties (surface tension, kinetics of atomic attachment, etc.). Mullins and Sekerka were the first to incorporate surface tension in a linear morphological stability analysis of growing crystals in a supercooled liquid [21]. Under the assumptions of local equilibrium and quasi-steady evolution, they investigated the behavior of an infinitesimal perturbation of a spherical solid by a single spherical harmonic. They found that the perturbation can decrease in time (stable growth) or increase in time (unstable growth) depending on the size of the precipitate, such that above a critical radius, the perturbation grows. Mullins and Sekerka [21] also identified the possibility of growing crystals with compact shapes when the supercooling is kept sub-critical by interparticle interactions. This was not quantified further, however. Coriell and Parker showed similar results hold for a growing cylinder [22]. Further, Coriell and Parker studied the stability of a solid sphere when finite attachment kinetics at the interface are included in the model. They showed that kinetics can enhance the stability [23], but when the size of the crystal increases, this effect decreases and the evolution is unstable. The Mullins–Sekerka instability leads to a wide variety of morphologies. For example, in the absence of anisotropy (or small anisotropy), Jacob proposed that the repeated tip-splittings dominate the shape of the interface and form dense branching morphologies [24,25], which are seen in experiments in a Hele-Shaw cell [26,27].

To grow compact crystals, the Mullins–Sekerka instability has to be suppressed. Recently, Cristini and Lowengrub reconsidered the three-dimensional (3D) quasi-steady crystal growth problem studied originally by Mullins and Sekerka [21] and Coriell and Parker [23]. Using linear theory, they demonstrated that there exist critical conditions of an imposed far-field heat flux (rather than a far-field supercooling) such that the classical Mullins–Sekerka instability can be suppressed and that the morphologies of growing crystals can be compact and controlled [1,2]. Note that what we mean by flux in Refs. [1–3] and this paper is the integral flux applied at the far-field boundary, (see Eq. (4)). Cristini and Lowengrub even found conditions (based on linear theory) for which the nonspherical crystals may grow self-similarly. Cristini and Lowengrub [2] performed 3D adaptive, dynamical simulations that suggest the

existence of nonlinear self-similar shapes and that a prescribed crystal symmetry can be achieved even in the nonlinear regime of growth.

For an isolated quasi-steady evolving crystal, an imposed far-field heat flux J represents the rate of area (2D) or volume (3D) change in time. The heat flux and the supercooling ΔT are related by $J \sim -R\Delta T$ in 3D [2,11], and by $J \sim -\log(R_\infty/R)\Delta T$ in 2D where R_∞ is the radius of a large domain containing the crystal, R is the effective radius of the crystal (radius of a sphere with the same volume) and ΔT denotes the difference between the far-field temperature and the phase change temperature for a flat interface [2,11]. Thus, conditions of specified flux can be enforced by varying ΔT with the crystal radius.

Very recently, we extended the studies of Cristini and Lowengrub and developed a nonlinear theory of self-similar crystal growth and melting [3]. Because the analysis is qualitatively independent of the number of dimensions, we focused on a perturbed 2D circular crystal growing or melting in a liquid ambient. We demonstrated that there exist nonlinear self-similar shapes with k-fold dominated symmetries. In the isotropic case, k is arbitrary and only growing solutions exist. When the surface tension is anisotropic, k is determined by the form of the anisotropy and both growing and melting solutions exist.

In this paper, we perform a stability analysis for 2D, noncircular self-similar crystals with isotropic surface tension growing in a supercooled melt, as found in our previous work [3]. We characterize the nonlinear morphological stability of the self-similar crystals, using a new spectrally accurate 2D boundary integral method in which a novel time and space rescaling is implemented [2]. This enables us to accurately simulate the long-time, nonlinear dynamics of evolving crystals. Our analysis and simulations reveal that self-similar shapes are stable to perturbations of the critical flux for self-similar growth in the sense that the symmetry of the crystal remains unchanged. This suggests that in experiments, small oscillations in the critical flux will not change the main features of self-similar growth. Shape perturbations may either grow or decay. However, at long times there is nonlinear stabilization even though unstable growth may be significant at early times. Interestingly, this stabilization leads to the existence of universal limiting shapes. That is, we find that the morphologies of the nonlinearly evolving crystals tend to limiting shapes that evolve self-similarly and depend only on the flux. A number of limiting shapes exist for each flux (the number of possible shapes actually depends on the flux), but only one is universal in the sense that a crystal with an arbitrary initial shape will evolve to this shape. The universal shape can actually be retrograde so that a portion of the interface may be melting during growth.

By performing a series of simulations, we construct a phase diagram that reveals the relationship between the applied flux and the achievable symmetries of the limiting shapes. Finally, we use the phase diagram to design a protocol by which the compact growth of crystals with desired symmetries can be achieved. Because our analysis shows that interactions among the perturbation modes are similar in both 2D and 3D, once the difference between the 2D and 3D heat fluxes (i.e. area vs. volume growth) is scaled out [3], our results apply qualitatively to 3D.

During crystal growth, there is at least one other example we are aware of in which the evolution of an arbitrary shaped crystal tends to a nonspherical limiting self-similar shape. In this example the velocity of the crystal is determined locally by the surface energy and the limiting shape is characterized by the Wulff shape [28,29]. The relevance of this example to our work is currently under study. In our case, the evolution is much more complicated since the velocity is determined nonlocally by the solution of the diffusion equation and multiple limiting morphologies are observed that depend on the flux. We note that during melting, Glicksman et al. [14] developed a quasi-static theory to describe self-similar melting of prolate spheroids in the absence of surface tension. Further self-similar two-fold symmetric solutions were found by Ham [30], and Horvay and Cahn [31] also in the absence of surface tension.

This paper is organized as follows: in Section 2, we review the governing equations, linear stability analysis and nonlinear self-similar theory; in Section 3, we present the numerical scheme; in Section 4, we discuss numerical results; and in

Section 5, we give conclusions and describe work in progress.

2. The theory

2.1. Governing equations

We consider a 2D solid crystal growing quasi-statically in a supercooled liquid phase. The interface Σ separates the solid phase Ω_1 from the liquid phase Ω_2. We assume that for simplicity the surface tension along the interface is isotropic, local equilibrium holds at the interface, and the thermal diffusivities of the two phases are identical. The results apply more generally however [32]. Using the nondimensionalization given in Refs. [1,2] in which the length scale is the equivalent radius of the crystal at time $t=0$ and the time scale is the characteristic surface tension relaxation time scale, the following nondimensional equations govern the growth of the crystal:

$$\nabla^2 T_i = 0 \quad \text{in } \Omega_i, \quad i=1,2, \tag{1}$$

$$V = (\nabla T_1 - \nabla T_2)\cdot \mathbf{n} \quad \text{on } \Sigma, \tag{2}$$

$$T_1 = T_2 = -\kappa \quad \text{on } \Sigma, \tag{3}$$

$$J = \frac{1}{2\pi}\int_{\Sigma} V \,\mathrm{d}s \tag{4}$$

and the interface Σ evolves via

$$\mathbf{n}\cdot\frac{\mathrm{d}\mathbf{x}}{\mathrm{d}t} = V \quad \text{on } \Sigma, \tag{5}$$

where T_i is the temperature field, $i=1$ for solid phase and $i=2$ for liquid phase, V is the normal velocity of the interface, $\mathbf{n}$ is the unit normal directed towards Ω_2, κ is the curvature, and J is the integral far-field heat flux and specifies the time derivative of the area of the solid phase.

2.2. Review of linear theory

Consider a circular crystal/melt interface perturbed by a linear combination of Fourier modes

$$r(\theta,t) = R(t) + \sum_{k=2}^{\infty} \delta_k(t)\cos k\theta, \tag{6}$$

where $R(t)$ is the radius of a underlying growing circle ($R(0)=1$) and the $\delta' s$ are amplitudes of perturbations. Note that in Eq. (6), $k=1$ means a translation of a circle (i.e. no shape perturbation occurs); the shape perturbation δ_2/R induced by the $k=2$ mode is stable for any finite flux (the amplitude δ_2 does not change in time) (see Eq. (9)). The rate of area growth for the unperturbed circle is

$$R(t)\frac{\mathrm{d}R}{\mathrm{d}t} = J(t), \tag{7}$$

where $J(t)$ is the specified flux. A classical linear stability analysis [33,11,3] yields the growth rate of the kth mode perturbation,

$$\left(\frac{\delta_k}{R}\right)^{-1}\frac{\mathrm{d}}{\mathrm{d}t}\left(\frac{\delta_k}{R}\right) = \frac{(k-2)(J-J_k)}{R^2}, \tag{8}$$

where the critical flux is

$$J_k(t) = \frac{C_k}{R(t)}$$

with the linear flux constant

$$C_k = \frac{2k(k^2-1)}{k-2}. \tag{9}$$

Note that with flux specified, the far field temperature is

$$T_\infty(t) = -J\,\log\left(\frac{R_\infty}{R}\right) - 1/R, \tag{10}$$

where R_∞ is the radius of a large domain containing the crystal. Eq. (8) shows that perturbations grow (decay) for $J>J_k$ ($J<J_k$). When $J=J_k$, the critical flux, the perturbation, relative to the underlying circle, is unchanged in time and the crystal grows self-similarly (at the level of linear theory). Hence in 2D, taking a constant flux $J>0$ results in the instability of perturbations with successively higher wavenumbers as the crystal grows, since $J_k \sim 1/R$. This is the Mullins–Sekerka instability [21].

Eqs. (7)–(10) are qualitatively similar to those obtained by Cristini and Lowengrub [1] in 3D. As discussed in Ref. [1], the critical flux in 3D is independent of R, which implies that the Mullins–Sekerka instability in 3D can be suppressed by taking a constant far-field flux $J>0$, since no

new unstable modes are created during the evolution. In contrast, Eqs. (8) and (9) show that in 2D, Mullins–Sekerka instability can be suppressed if the 2D far-field flux decreases as $J \sim 1/R$. This difference exactly reflects the different scaling of the flux between 2D and 3D (area vs. volume evolution). If one rescales the far-field flux J by R, i.e. $\tilde{J} = RJ$, then $R^2(\mathrm{d}R/\mathrm{d}t) = \tilde{J}$ and the right-hand side of Eq. (8) becomes $(k-2)(\tilde{J} - C_k)/R^3$. These equations are identical to those obtained in 3D if C_k is replaced by J_k^{3D} and the 3D far-field flux is $\tilde{J}$ [1]. This suggests that our 2D work applies qualitatively to the 3D problem.

Let us now determine the flux for which the kth mode has the largest growth rate. This is important if the shape of the interface is a mixture of Fourier modes since the fastest growing mode will dominate the shape. As in Ref. [2], we will exploit this idea later to control the shapes of growing crystals with desired symmetries. Following Ref. [1], we get

$$J_k^*(t) = \frac{6k^2 - 2}{R(t)}. \tag{11}$$

Further, from $J_k^*(t)$, we can determine the mode q that marks the upper bound of the band of unstable modes. To find q, we equate $J_k^* = J_q$ (replace k in Eq. (9) by q), so that mode q has zero growth rate (i.e. $q-1$ is the largest unstable mode) if the applied flux is set to J_k^*. A remarkable feature is that the $q(k)$ and the 3D analogue given in Ref. [1] are nearly identical even though the $q(k)$ are (positive) roots of different cubic polynomials in 2D and 3D. This agreement suggests the modes interact with each other in a similar manner for both 2D and 3D when the flux is rescaled by R.

2.3. Review of nonlinear theory

In the nonlinear theory we have recently developed [3], we represent the temperature field through a single-layer potential. This yields the first kind Fredholm integral equations [34,35] for $V(\mathbf{x}, t)$ and $T_\infty(t)$, which are the normal velocity of the interface Σ and the far-field temperature, respectively:

$$-\kappa(\mathbf{x}, t) = \int_{\Sigma(t)} G(\mathbf{x} - \mathbf{x}') V(\mathbf{x}', t)\, \mathrm{d}s(\mathbf{x}') + T_\infty(t), \tag{12}$$

$$J(t) = \frac{1}{2\pi} \int_{\Sigma(t)} V(\mathbf{x}', t)\, \mathrm{d}s(\mathbf{x}'), \tag{13}$$

where $G(\mathbf{x}) = (1/2\pi)\log|\mathbf{x}|$ is the Green's function.

A fundamental feature of self-similar evolution is that time and space are separable, i.e.

$$\mathbf{x}(s, t) = R(t)\tilde{\mathbf{x}}(s), \tag{14}$$

where $\tilde{\mathbf{x}}(s)$ specifies the self-similar shape, $R(t)$ is a scaling function related to the effective radius of the growing crystal, and s is the arclength along the self-similar interface. Substituting Eq. (14) into Eq. (12) and using Eq. (13), then differentiating the resulting equation with respect to arclength gives [3]

$$(-\tilde{\kappa})_s / \mathscr{G}[\tilde{\mathbf{x}}]_s = JR\frac{\pi}{\tilde{A}} = C^{\mathrm{NL}}, \tag{15}$$

where the notation $(.)_s = \partial/\partial s$, C^{NL} is a constant in space and time (from separation of variables) and is referred to as the nonlinear heat flux constant. Further,

$$\mathscr{G}[\tilde{\mathbf{x}}](s) = \int_{\tilde{\Sigma}} \tilde{\mathbf{x}}' \cdot \mathbf{n}(\tilde{s}') G(\tilde{\mathbf{x}}(s) - \tilde{\mathbf{x}}(s'))\, \mathrm{d}s'. \tag{16}$$

The above system is identical to the 3D system for nonlinear self-similar crystal shapes if the constant C^{NL} is replaced by the 3D nonlinear self-similar flux, G is replaced by the 3D Green's function and $\tilde{T}_\infty(t)$ is defined appropriately [32]. This further supports our contention that 2D analysis can provide insight to 3D evolution.

In Ref. [3], we used a quasi-Newton method to solve the system of equations numerically to determine the heat flux constant and the self-similar solution. Our numerical results revealed that there exist nonlinear self-similar shapes with k-fold dominated symmetries. An amplitude-dependent nonlinear heat flux constant C_k^{NL} is associated with each shape; for small-amplitude perturbations of the cylindrical state C_k^{NL} tends to the linear flux constant C_k in Eq. (9). In the

isotropic case, k is arbitrary and only growing solutions exist. Moreover, in a k-fold dominant self-similar shape, only mode k and its harmonics (integer multiples of the wavenumber k) appear in the Fourier series description of the interface. We also find that one of the effects of nonlinearity is to reduce the nonlinear critical flux compared to that predicted by linear theory.

3. Boundary integral method with time and space rescaling

In order to test the stability of self-similar solutions we found in Ref. [3], we develop a scheme to investigate the long-time, fully nonlinear evolution of a crystal. Following Ref. [2], we introduce the spatial and temporal scaling of the dynamical equations

$$\mathbf{x} = \bar{R}(\bar{t})\bar{\mathbf{x}}(\bar{t},\alpha), \tag{17}$$

$$\bar{t} = \int_0^t \frac{1}{R(t')^3}\,\mathrm{d}t', \tag{18}$$

where $\bar{R}(\bar{t}) = R(t(\bar{t}))$ and $\bar{\mathbf{x}}(\bar{t},\alpha)$ is the position vector of the scaled interface, and $\bar{t}$ is the new time variable. The scaling $\bar{R}$ is chosen such that the area $\bar{A}$ enclosed by the scaled interface is constant in time. The scaling $\bar{R}$ can be found by integrating the normal velocity over the interface and dividing by 2π to get

$$J = \frac{\bar{A}}{\pi}\frac{1}{\bar{R}^2(\bar{t})}\frac{\mathrm{d}\bar{R}(\bar{t})}{\mathrm{d}\bar{t}}. \tag{19}$$

The normal velocity in the new frame is $\bar{V}(\bar{t},\alpha) = \partial\bar{\mathbf{x}}(\bar{t},\alpha)/\partial\bar{t}\cdot\mathbf{n}$ and satisfies

$$-\bar{\kappa} - \bar{J}\mathscr{G}[\bar{x}] = \int_{\bar{\Sigma}} G(|\bar{\mathbf{x}} - \bar{\mathbf{x}}'|)\bar{V}\,\mathrm{d}s' + \bar{T}_\infty(\bar{t}) \tag{20}$$

and

$$0 = \int_{\bar{\Sigma}} \bar{V}\,\mathrm{d}s, \tag{21}$$

where

$$\bar{J} = \frac{\pi\bar{R}J}{\bar{A}} = \frac{\mathrm{d}}{\mathrm{d}\bar{t}}\log(\bar{R}(\bar{t})) \quad \text{and } \bar{\kappa} = \bar{R}\kappa.$$

Thus the scaling factor is

$$\bar{R}(\bar{t}) = \exp\left(\int_0^{\bar{t}} \bar{J}\,\mathrm{d}\bar{t}'\right). \tag{22}$$

Further, in Eq. (20) we have taken

$$\bar{T}_\infty(\bar{t}) = \frac{\bar{A}\,\log(\bar{R})}{\pi}\,\bar{J} + T_\infty(t(\bar{t}))\bar{R}(\bar{t}),$$

and $\mathscr{G}(\bar{\mathbf{x}}) = \int_{\bar{\Sigma}} \bar{\mathbf{x}}'\cdot\mathbf{n}(\bar{\mathbf{x}}')G(\bar{\mathbf{x}} - \bar{\mathbf{x}}')\,\mathrm{d}s'$. Note that Eq. (20) reduces to the self-similar Eq. (15) when the normal velocity $\bar{V} = 0$.

To evolve the interface numerically, Eqs. (20) and (21)) are discretized in space using spectrally accurate discretizations and a scaled (equal arclength) parametrization [36]. The resulting discrete system is solved efficiently using GMRES together with a diagonal preconditioner in Fourier space [36,37]. Once $\bar{V}$ is obtained, the interface is evolved by using a second order accurate nonstiff updating scheme in time [36].

4. Results and discussions

4.1. Stability analysis

4.1.1. Stability analysis with respect to flux perturbations

In this section, we study the stability of a self-similar shape by perturbing the flux constant and analyzing the resulting evolution of the shape using the nonlinear time evolution scheme presented in Section 3. As a representative example, we consider an eight-fold symmetric self-similar shape with a shape factor $\delta/R = 0.0284$ and flux constant $C_8^{\mathrm{NL}} = 165.38104$ (see the inset in Fig. 3(a) labeled unperturbed). The shape factor is defined as

$$\delta/R = \max||\tilde{\mathbf{x}}|/\tilde{R}_{\mathrm{eff}} - 1|, \tag{23}$$

where $\tilde{\mathbf{x}}$ is the position vector from the centroid of the shape to the interface and $\tilde{R}_{\mathrm{eff}}$ is the effective radius of the nonlinear (self-similar) shape.

In Fig. 1(a), we use a sine wave to perturb the flux constant

$$\bar{J} = C_8^{\mathrm{NL}}(1 - \mathscr{A}\,\sin(2\pi\omega t))\frac{\pi}{\bar{A}}, \tag{24}$$

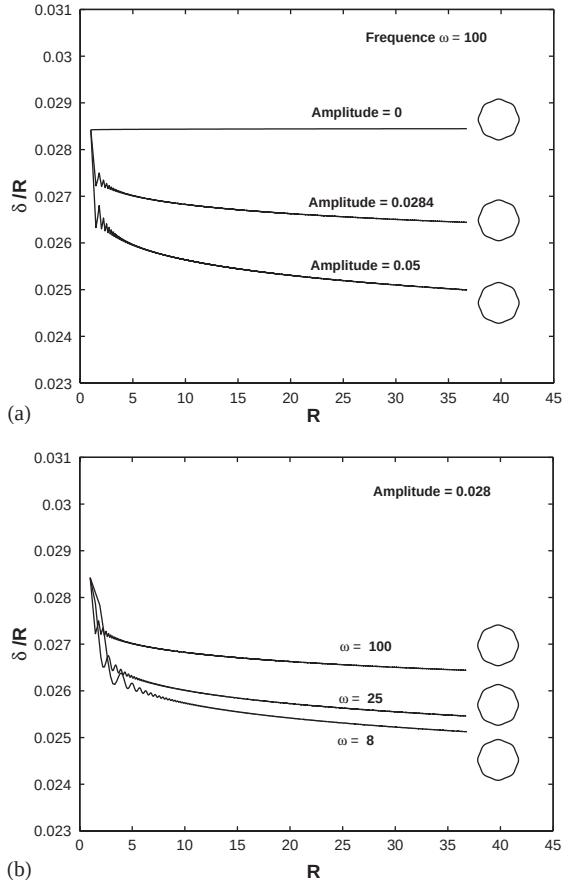

Fig. 1. Effect of flux perturbations. (a) evolution of shape factor δ/R for a crystal with eight-fold symmetry when the flux constant is perturbed by a sin wave with different amplitudes (as indicated) through Eq. (24) with frequency $\omega = 100$. Associated morphologies shown as insets and (b) shape factor when the flux constant is perturbed by a sin wave with different frequencies through Eq. (24) with amplitude $\mathscr{A} = 0.0284$.

where $\mathscr{A}$ is the perturbation amplitude, ω is the frequency and $\bar{A}$ is the area of the self-similar shape. The self-similar shape is then used as initial data and is evolved using the flux from Eq. (24). In this calculation, we take $\omega = 100$ and consider perturbation amplitudes, $\mathscr{A} = 0.0,\ 0.0284,\ 0.05$. When the perturbation amplitude increases, the final shape deviates more from the original self-similar shape. At early growth times, δ/R varies rapidly. At later times, the shape stabilizes (δ/R tends to a nonzero constant) as the size of the crystal grows larger. This is likely because the overall flux $J \sim \bar{J}/R(t)$ decreases as crystal grows making the crystal less sensitive to variations in $\bar{J}$ at large radii.

Alternatively, in Fig. 1(b), we take $\mathscr{A} = 0.0284$ and perturb the flux constant with different frequencies $\omega = 100,\ 25,\ 8$. Observe that the deviation of shape factor δ/R from the original self-similar shape decreases with increasing perturbation frequency. This is because the time scale for flux oscillations $\sim 1/\omega$ becomes much larger than the time scale for growth when the frequency ω is large. As before the shape tends to stabilize as the crystal radius increases although it appears to take a longer time to do so particularly for the low-frequency perturbations.

These two results strongly suggest that self-similar evolution is stable with respect to flux perturbations in the sense that symmetry of the crystal remains unchanged. These results are generic in that the conclusions hold for other self-similar shapes. Further, these results have important implications for an experimental investigation of self-similar growth, since in experiments it may be difficult to precisely control the far-field flux (via the far-field temperature).

4.1.2. Stability analysis with respect to shape perturbations

We next study the morphological stability of self-similar crystals by adding an arbitrary trigonometric perturbation. The perturbed shapes are then used as initial data for simulations of nonlinear evolution. The flux is taken from the result of the Quasi-Newton solver for the original self-similar shape. The new time-space rescaling scheme presented in Section 3 (effective crystal radius grows exponentially in the new time variable) enables us to investigate the shape evolution for very large R (much larger than has been previously possible) and hence completely allows us to characterize the stability of the perturbation.

4.1.2.1. Self-similar shapes with four fold symmetry. We consider a four fold isotropic self-similar shape with shape factor $\delta/R = 0.028$ and flux constant $C_4^{\mathrm{NL}} = 59.87$ (see inset in Fig. 2(a) labeled

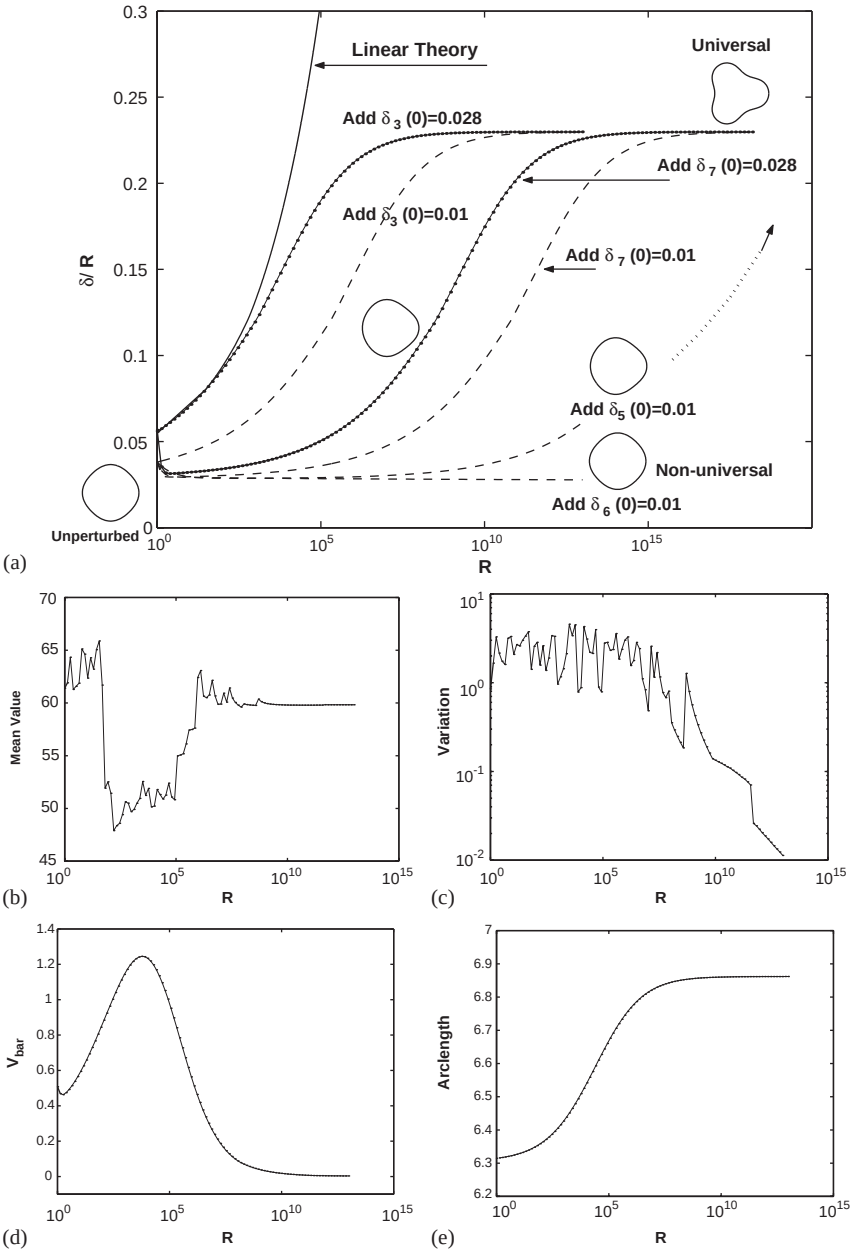

Fig. 2. Effect of shape perturbations and evolution to a universal shape: (a) shape factor evolution and associated morphologies of a four-fold self-similar shape (shown in an inset labeled unperturbed) with $\delta/R = 0.028$ (and flux constant $C_4^{\mathrm{NL}} = 59.87$) from Li et al. [3] perturbed by adding a single mode with different wavenumbers and amplitudes as indicated. The flux constant is taken to be C_4^{NL}. Linear theory overpredicts the growth of the perturbation as indicated in the figure. For generic perturbations, the nonlinear evolution tends to a universal limiting shape with a three-fold symmetry and shown in the upper right corner of (a). A nonuniversal four-fold limiting shape (lower right of (a)) is obtained when the shape is perturbed by adding mode 6. The mode 5 perturbation will tend to the universal shape at longer times (larger R). In (b)–(e), evidence is shown that the three-fold universal shape is a self-similar solution and satisfies Eq. (15) with $C^{\mathrm{NL}} = C_4^{\mathrm{NL}} = 59.87$. (b) The mean value of Eq. (15) during the evolution. (c) The maximum deviation from the mean value of Eq. (15). (d) The maximum normal velocity at different crystal sizes R. (e) The evolution of interface arclength (in the scaled frame).

unperturbed). In Fig. 2(a), the evolution of the shape factors δ/R is shown versus radius R for different perturbation modes and amplitudes. For this case, linear theory describing the evolution of perturbations of a circle (see Section 2) predicts that only mode 3 is unstable for the flux constant $C_4^{NL} = 59.87$. This linear theory typically over-predicts the growth of perturbations as indicated in the figure.

In general, and beyond the prediction of linear theory, there is nonlinear stabilization and perturbations eventually stop growing. For generic perturbations, the nonlinear evolution tends toward a single universal limiting shape with a three-fold symmetry (for this value of flux), which is shown in the upper right corner of Fig. 2(a). In this case, a generic (arbitrary) perturbation requires at least one odd perturbation mode, so that all modes are eventually produced through nonlinear interactions. Note that the time required to reach this universal three-fold shape depends strongly on the initial perturbation. On the other hand, for special perturbations (e.g. perturbations containing only even modes), the evolution tends toward a non-universal limiting shape with four-fold symmetry, as shown in the inset in the lower right of Fig. 2(a), where the initial shape is perturbed by adding mode 6.

As shown below, both the universal and nonuniversal limiting shapes are actually nonlinear solutions of the self-similar crystal growth Eq. (15) with the same flux constant C_4^{NL}. However the nonuniversal shapes are unstable in the sense that if they are perturbed by adding arbitrary wave-numbers (which by definition contain odd modes), the perturbations will grow and the shape will tend towards the universal three-fold shape. Linear theory predicts that mode 3 is the fastest growing mode for this specific flux C_4^{NL}, and this is reflected in the three-fold symmetry of the universal shape. However, linear theory *does not* predict the existence of the universal shape. The existence of limiting shapes is a surprising fully nonlinear result.

Fig. 2(a) strongly suggests that the limiting shapes, both the universal three-fold shape and the nonuniversal four-fold shape, are actually self-similar solutions of the Eq. (15) in Section 2.3. Here we present evidence that this is indeed the case. We consider the universal three-fold shape, though similar results hold for the nonuniversal shape. This new self-similar solution deviates much more from the circle than those we found previously [3].

In Figs. 2(b)–(e), we plot data from the three-mode initial perturbation with $\tilde{\delta}_3(0) = 0.028$ as a typical example. In Fig. 2(b), the mean value of the flux constant C^{NL} from the ratio in the left-hand side of Eq. (15) is shown versus R throughout the evolution. This ratio should be constant for a self-similar shape and should be equal to the applied far-field flux constant $C_4^{NL} = 59.87$. The mean value approaches a constant as is consistent with self-similar evolution. The value of the mean $C_{mean} = 59.83$ at $R = 10^{12}$ is slightly smaller than the applied flux with flux constant $C_4^{NL} = 59.87$. We next calculate the maximum deviation of C^{NL} from C_{mean}^{NL} (i.e. $\max(|C^{NL} - C_{mean}^{NL}|)$ as a function of R. This is shown in Fig. 2(c) where it is seen that the maximum deviation is indeed decreasing, especially at later times. The deviation at $R = 10^{12}$ is on the same order as the difference between C_{mean}^{NL} and C_4^{NL}. As further evidence of self-similarity, we plot the maximum normal velocity (i.e. $\max|\bar{V}|$) as a function of radius R in Fig. 2(d). The normal velocity $\bar{V}$ tends to zero as R increases which is consistent with the self-similar evolution of the limiting shape. Finally, in Fig. 2(e), we plot the arclength of the interface (in the rescaled reference frame used for computation) versus R and observe that the arclength becomes constant indicating that the shape stops changing. Since the surface tension is isotropic, this also provides a measure of the surface energy in the scaled frame.

Putting all of this direct quantitative evidence together strongly suggests that the limiting shapes are self-similar. Furthermore since the universal three-fold shape is stable and can be achieved by evolving arbitrary perturbations, it is an attractor for the evolution. Although it is possible to dynamically achieve a four-fold nonuniversal limiting shape, this shape is not stable to arbitrary perturbations and can only be achieved by evolving special mode combinations (e.g. even modes).

4.1.2.2. Self-similar shapes with eight-fold symmetry. In the previous section, we have analyzed the stability of a perturbed self-similar shape with a four-fold symmetry and demonstrated the existence of limiting shapes. We now extend this analysis by examining the stability of an eight-fold self-similar shape from Section 4.1.1 (see the inset in Fig. 3(a) labeled unperturbed) with $\delta/R = 0.0284$ and $C_8^{NL} = 165.38104$. With this flux constant, modes 3–7 are linearly unstable. Thus, it is reasonable to expect that a larger number of limiting shapes exist compared to the case considered in the previous section. Note that the flux C_8^{NL}/R for the eight-fold symmetric self-similar shape is close to $J_5^*(t) = 148/R(t)$, from Eq. (11), which is the flux such that mode 5 has the fastest growth rate according to linear theory.

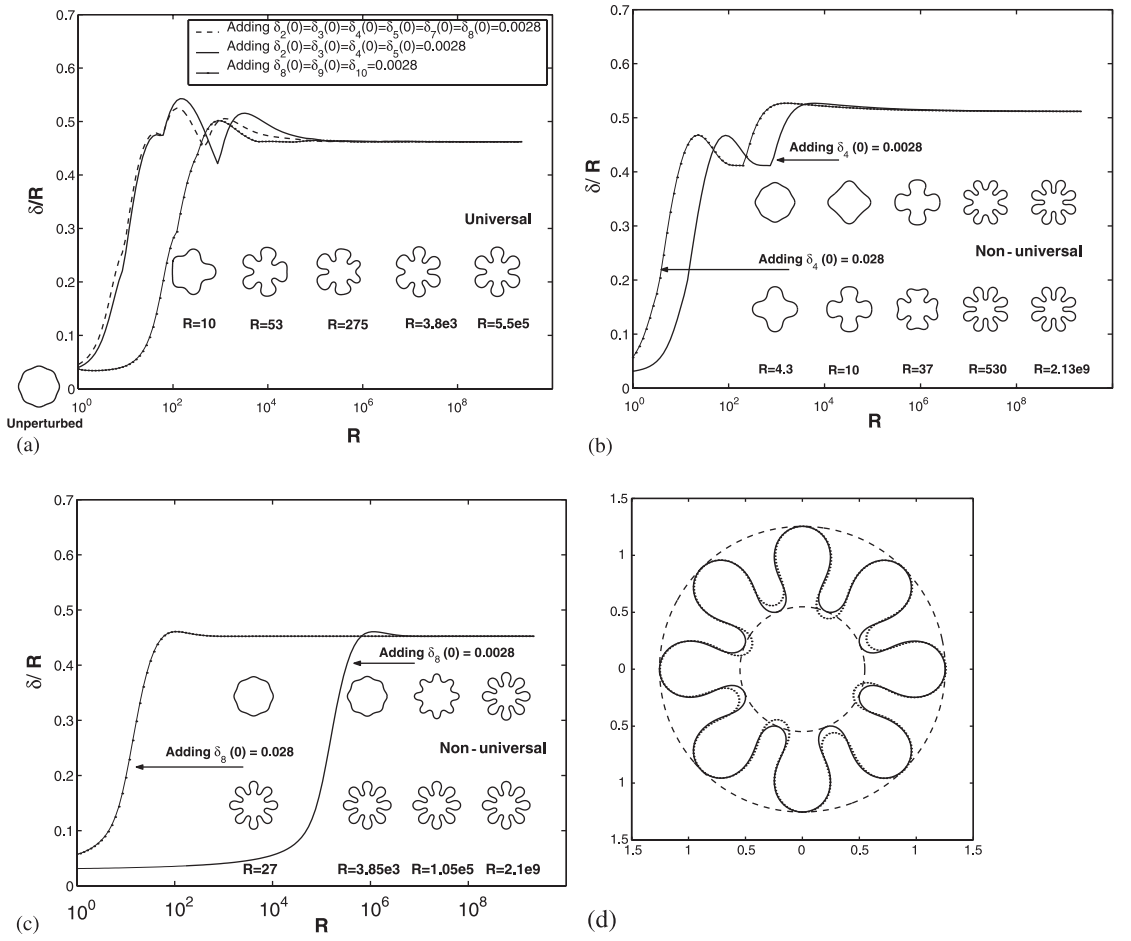

Fig. 3. The effect of shape perturbations on an eight-fold self-similar shape (shown in an inset) with $\delta/R = 0.028$ and flux constant $C_8^{NL} = 165.38$ from Li et al. [3]: (a) Shape factor evolution is shown for perturbations of the original self-similar shape with combinations of modes with different wavenumbers and amplitudes as indicated. The associated morphologies are shown for the solid curve as a representative example. The flux constant is taken to be C_8^{NL}. The evolution tends to a universal limiting shape with a six-fold symmetry. (b) and (c) show that the evolution also may tend to two nonuniversal shapes each with an eight-fold symmetry depending on the initial shape. In (b) the original self-similar shape is perturbed by adding mode 4 with amplitudes as indicated. Both the four-fold and eight-fold symmetries remain throughout the evolution. In (c), the original shape is perturbed by adding mode 8 with different amplitudes. (d) shows a comparison between the two eight-fold nonuniversal limiting shapes. Remarkably, the fingers are the same and it is the troughs that differ.

In Fig. 3(a) the shape factor is shown versus R for perturbations of the original self-similar shape with combinations of modes with different wavenumbers and amplitudes as indicated. The associated morphologies are shown for the solid curve as a representative example. The evolution is highly nonlinear and, as in the lower symmetry simulations shown in the previous section, there is nonlinear stabilization during growth. The nonlinear stabilization seems to characterize the process of "finger" competition (i.e. generation, retraction and tip-splitting) and the associated formation of channels between neighboring "fingers" as seen in the sequence of evolving morphologies.

At early times (small R), mode 5 dominates the shape in agreement with the prediction of linear theory. However, when R increases, certain fingers of the five-fold shape experience a complex process of tip-splitting, finger shrinking and tip re-splitting. Eventually, mode 6 emerges and the evolution tends toward a single six-fold universal limiting shape with identical fingers as indicated in the figure. An analysis (not presented) similar to that given in the previous section strongly suggests this limiting shape evolves self-similarly. Interestingly, the six-fold universal shape is retrograde and thus cannot be parametrized by the polar angle. Moreover, the evolution (not shown) of the arclength in the scaled frame is nonmonotone as a function of R due to the complex shape transitions.

Next, consider special perturbations of the original eight-fold self-similar shape by adding modes 4 and 8 in Figs. 3(b) and (c), respectively. The evolution tends toward two different eight-fold nonuniversal, retrograde limiting shapes. The limiting shape obtained from the 4 mode perturbation retains the four-fold symmetry even though 8 fingers are present. In contrast, the limiting shape from the 8 mode perturbation retains only the eight-fold symmetry. A detailed comparison of the shapes is shown in Fig. 3(d), where the thick solid line is the limiting shape for the mode 8 perturbation and the dots correspond to the mode 4 perturbation (we rotate the limiting shape in Fig. 3(b) by $\pi/8$). Observe that the fingers are identical but the troughs are different.

As another example of a special perturbation, the eight-fold self-similar shape can be perturbed by adding mode 7. In this case (not shown), the evolution tends toward a seven-fold nonuniversal, retrograde limiting shape with identical fingers.

In summary, our stability analysis reveals the existence of limiting shapes with six-, seven- and eight-fold symmetries when the flux constant is equal to C_8^{NL}, with the six-fold limiting shape being universal in the sense that arbitrary perturbations will eventually lead to this shape. Putting this together with our results from stability analysis for the four-fold self-similar shapes suggests that the universal limiting shapes depend only on the flux while the nonuniversal shapes depend also on the initial data. Next we explore the relation between the flux and the achievable limiting shapes.

4.1.2.3. Limiting shape phase diagram. The simulations in the previous sections demonstrate the importance of far-field flux on the selection of limiting shapes. Here, we bring together these results and construct a limiting shape phase diagram which is shown in Fig. 4(a). In this figure, we plot the symmetry mode k of the limiting shapes versus corresponding flux constants C, i.e. the flux $J = C/\bar{R}$.

The set of symmetries of the dynamically achievable limiting shapes found in this paper lies in Region II and roughly corresponds to those modes that have growth rates between 0 (upper dashed curve) and the maximum growth rate (lower dashed curve) as predicted by linear theory. There may be several shapes with a given symmetry k and flux constant C (see Fig. 3(b) and (c)). Region II is bounded below by a piecewise constant curve that describe the relation between the observed symmetries of the universal limiting shape and the flux constant. The stars denote actual simulation data. The upper bound of region II is the piecewise constant curve obtained from the nonlinear simulations of self-similar shapes by Li et al. [3]. The dot-dashed curve is a fit to numerical data from Li et al. [3]. We cannot rule out the possibility of the existence of limiting shapes in region I but we have not as yet been able to compute them.

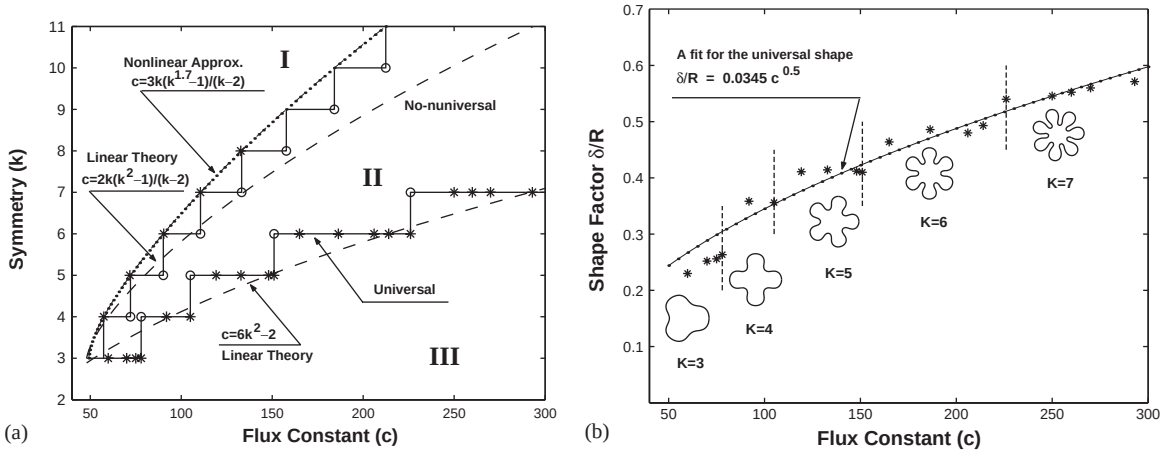

Fig. 4. (a) Limiting shape phase diagram. The set of dynamically achievable shapes is found to be Region II. There may be several shapes with a given symmetry k and flux constant C (see Fig. 5(b) and (c)). Region II is bounded by two piecewise constant curves that describe the relation between the observed symmetries of the limiting shape and the flux constant. The stars denote actual simulation data. The universal limiting shapes lie on the lower piecewise constant curve. The upper piecewise constant curve is obtained from the nonlinear simulations of self-similar shapes in Li et al. [3]. In between these curves, nonuniversal shapes may occur with finite multiplicity. The dot-dashed curve is a fit to that numerical data from Li et al. [3]. The dashed curves correspond to predictions of linear theory and are shown for reference. The upper dashed curve shows the relation between the flux constant and the mode with zero growth rate (i.e. self-similar). The lower dashed curve shows the relation between the flux constant and the fastest growing mode. (b) The associated shape factors of the universal limiting shapes. The solid-dotted curve suggests that the asymptotic behavior may be $\delta/R \sim \sqrt{C}$ at large flux constants C. The vertical dashed lines indicate transitions from symmetry k to $k+1$. Representative universal morphologies are shown for each symmetry.

In between these piecewise constant curves, nonuniversal shapes may occur with finite multiplicity. The dashed curves correspond to predictions of linear theory and are shown for reference. The upper dashed curve shows the relation between the flux constant and the mode with zero growth rate (i.e. self-similar). The lower dashed curve shows the relation between the flux constant and the fastest growing mode. Note that while linear theory does not predict the existence of a universal limiting shape, linear theory prediction for the fastest growing mode does provide a good estimate for the symmetry of the universal limiting shape.

To produce the phase-diagram, the limiting shapes are found by performing simulations with a variety of initial shapes and the specified flux constant. The curves marking the upper and lower bounds of region II takes a staircase pattern because there are morphology transitions from k-fold to $k+1$-fold symmetries. The circles mark the transitions. The accuracy in the jumps on the universal curve is calculated to be within 5%. The jumps on the upper curve are only approximate. On the universal curve, the length of each step increases as the flux constant increases indicating that larger and larger fluxes are needed to produce higher and higher symmetries of the universal shapes. Notice that there is a continuous set of flux constants that can be used to achieve a limiting (but not necessarily universal) shape of a particular symmetry. The shape factors δ/R of these limiting shapes are different, however. In addition, the time needed for an arbitrary initial shape to evolve to the limiting shape is larger for fluxes near the transition points than for fluxes in the interior of the set.

In Fig. 4(b) we examine the relation between the shape factors δ/R of the universal limiting shapes and the flux constant. The vertical dashed lines indicate transitions from symmetry k to $k+1$. Representative universal morphologies are shown for each symmetry. The solid-dotted curve suggests that the asymptotic behavior may be $\delta/R \sim$

$\sqrt{C}$ at large flux constants C. This reflects the fact that larger symmetries require larger fluxes to maintain as seen from the linear analysis of a perturbed circle. Larger fluxes, in turn, allow more modes to grow and result in larger shape perturbations. Our results suggests that the universal shapes with symmetries six-fold and higher are retrograde. Further, our results also suggest the intriguing possibility that there may be a critical value of C at which the topology of the universal shape changes from a simply connected to a multiply connected region characterized by a shape with identical, equally spaced fingers that are all connected at the origin (i.e. there is an inner tangent circle with vanishing radius). This is currently under study.

4.2. Application of phase diagram: shape control

The phase diagram discussed in the previous section can be used to design a nonlinear protocol that might be able to be carried out in a physical experiment to control the nonlinear morphological evolution of growing crystal. A less rigorous strategy based on linear theory was previously formulated in 3D by Cristini and Lowengrub [2].

The nonlinear protocol is as follows. From the diagram, we have the relation between symmetry of the universal limiting shape and the flux constant. By choosing the flux constant consistent with the diagram for a symmetry k, a crystal with an arbitrary initial shape will evolve to the corresponding k-fold limiting shape. To achieve the most rapid evolution towards the universal limiting shape, the flux constant should be chosen away from a symmetry transition. In this manner, the prescribed symmetry of the crystal is achieved in the shortest time. As seen in the phase diagram, using linear theory to determine the mode with maximum growth rate (lower dashed curve in the Fig. 4(a)) provides only an approximation of the fluxes needed to obtain the universal limiting shape. In fact, in the shape control experiment presented by Cristini and Lowengrub [2] the actual flux used was slightly smaller than that predicted by linear theory. This is consistent with our phase diagram.

In Fig. 5, we present shape factor evolution towards universal limiting shapes corresponding to

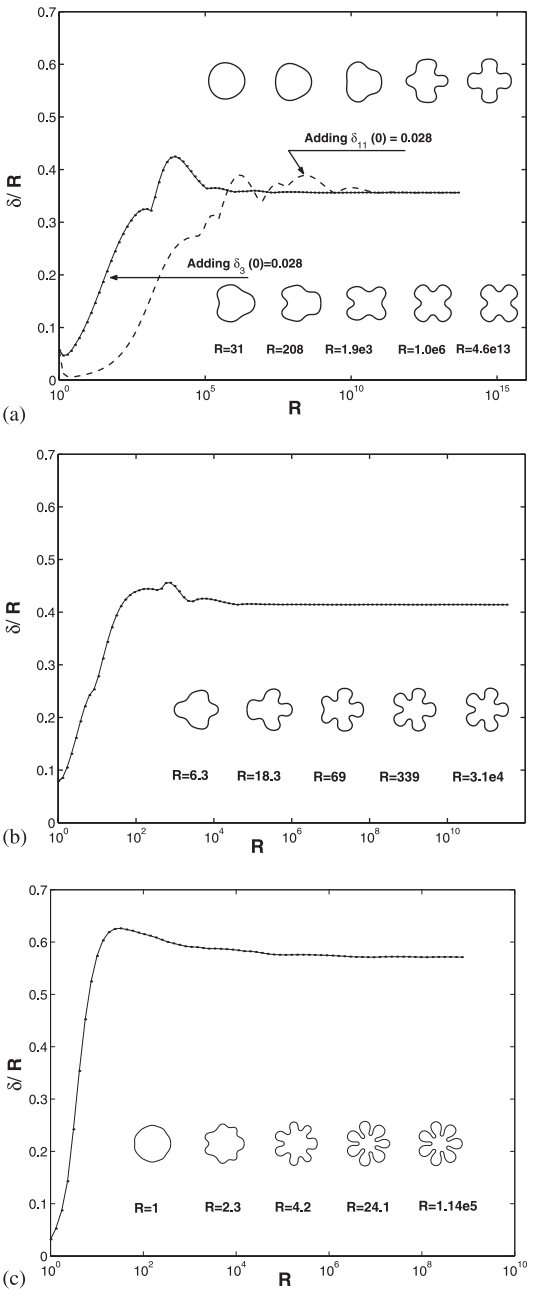

Fig. 5. Universal limiting shapes corresponding to different fluxes: (a) shows the evolution to a four-fold limiting shape using the flux constant $C = 105$; (b) shows the evolution to a five-fold limiting shape using the flux constant $C = 132.82$ and (c) shows the evolution to a seven-fold limiting shape using the flux constant $C = 292$.

different fluxes. The results are independent of the initial shape. Fig. 5(a) shows the evolution to a four-fold limiting shape using the flux constant $C = 105$. Fig. 5(b) shows the evolution to a five-fold limiting shape using the flux constant $C = 132.82$. Fig. 5(c) shows the evolution to a seven-fold limiting shape using the flux constant $C = 292$. Note that flux constant in Fig. 5(a) is close to a symmetry transition point and the evolution reaches the universal shape at a larger radius compared to Fig. 5(b) and Fig. 5(c) where the flux constants are located away from symmetry transitions.

5. Conclusion and future work

In this paper, we performed a stability analysis of 2D, noncircular self-similar crystals with isotropic surface tension growing in a supercooled melt. The existence of such self-similarly growing crystals was demonstrated recently in our previous work [3]. Here, we characterized the nonlinear morphological stability of the self-similar crystals, using a new spectrally accurate 2D boundary integral method in which a novel time and space rescaling is implemented [2]. This enabled us to accurately simulate the long-time, nonlinear dynamics of evolving crystals.

Our analysis and simulations revealed that self-similar shapes are stable to perturbations of the critical flux for self-similar growth, in the sense that the symmetry of the crystal remains unchanged. This suggests that in experiments, small oscillations in the critical flux will not change the main features of self-similar growth. Shape perturbations either grow or decay. However, at long times there is nonlinear stabilization even though unstable growth may be significant at early times. Interestingly, this stabilization leads to the existence of universal limiting shapes. That is, we found that the morphologies of the nonlinearly evolving crystals tend to limiting shapes that evolve self-similarly and depend only on the flux. A number of limiting shapes exist for each flux (the number of possible shapes actually depends on the flux), but only one is universal in the sense that a crystal with an arbitrary initial shape will evolve to this shape. The universal shape can actually be retrograde. By performing a series of simulations, we constructed a phase diagram that reveals the relationship between the applied flux and the achievable symmetries of the limiting shapes. Finally, we used the phase diagram to design a nonlinear protocol that might be able to be used in a physical experiment to control the nonlinear morphological evolution of growing crystal. Because our analysis shows that interactions among the perturbation modes are similar in both 2D and 3D, once the difference between the 2D and 3D heat fluxes (i.e. area vs. volume growth) is scaled out [3], our results apply qualitatively to 3D.

In our simulations, the limiting shape is achieved when the crystal grows very large compared with its initial size. Depending on the initial size, convective transport driven by buoyancy effects may become important. They are neglected here. However, this paper provides insight to nonlinear crystal growth by demonstrating that there is a wide variation (that depends on the flux and initial data) in the evolution to the limiting shape. For instance, starting from an arbitrary initial shape, there are certain fluxes such that the evolution to the limiting shape occurs over much shorter times (i.e. smaller crystal sizes) than other fluxes. This suggests that it may be feasible to control the shapes of growing crystals in an experiment following the protocol proposed here.

A natural question is whether the limiting shapes we have found here could have been directly obtained as extrema of an energy function in analogy with Wulff shapes that are obtained as equilibria for crystals with fixed volume [29]. Here, however, the system is open as heat is removed at the far-field. The relation between the limiting shapes and the system energy is currently under study.

We have also neglected some other important physical effects such as surface tension anisotropy and interface kinetics. These effects can play a central role in the development of the complex patterns seen during crystal growth by favoring certain directions of growth. We are currently investigating these physical effects and our results indicate that nonlinear, stable, self-similar shapes exist in this context as well [32]. This will be presented in a subsequent paper [38].

We are currently performing 3D simulations to confirm that our 2D model indeed captures the significant features of 3D growth. In future work, we will demonstrate that universal attractive 3D limiting shapes exist.

Finally, we will also investigate the implications of this work on the directional solidification of both pure materials and binary alloys. In particular, based on previous linear stability analysis of directional solidification (e.g. Ref. [39]), we conjecture that there may exist nonlinear limiting (and universal) interface profiles that can be achieved by careful control of the temperature gradients.

Acknowledgements

The authors thank Prof. Robert Sekerka for stimulating discussions. S. Li also thanks Prof. Vaughan Voller and Yubao Zhen for technical discussions. The authors also acknowledge the generous computing resources from the Minnesota Supercomputer Institute, the Network and Academic Computing Services at University of California at Irvine (NACS), and computing resources of BME department (U.C. Irvine) through a grant from Whitaker Foundation. S. Li is supported by a doctoral dissertation fellowship from University of Minnesota and by the Department of Biomedical Engineering and the Department of Mathematics at U.C. Irvine where he is a visiting researcher. J. Lowengrub and V. Cristini thank the National Science Foundation (Division of Mathematical Sciences) for partial support.

References

[1] V. Cristini, J. Lowengrub, J. Crystal Growth 240 (2002) 267.
[2] V. Cristini, J. Lowengrub, J. Crystal Growth 266 (2004) 552.
[3] S. Li, J. Lowengrub, P. Leo, V. Cristini, J. Crystal Growth 267 (2004) 703.
[4] J.S. Langer, Rev. Mod. Phys. 52 (1) (1980).
[5] G.B. McFadden, S.R. Coriell, R.F. Sekerka, Acta Mater. 48 (2000) 3177.
[6] G.B. McFadden, S.R. Coriell, R.F. Sekerka, J. Crystal Growth 208 (2000) 726.
[7] D.M. Anderson, G.B. McFadden, A.A. Wheeler, Physica D 151 (2001) 305.
[8] D.A. Kessler, H. Levine, Acta Metall. 36 (1988) 2693.
[9] T. Uehara, R.F. Sekerka, J. Crystal Growth 254 (2003) 251.
[10] B.K. Johnson, R.F. Sekerka, Robert Almgren, Phys. Rev. E 60 (1999) 705.
[11] L.N. Brush, R.F. Sekerka, J. Crystal Growth 96 (1989) 419.
[12] S.R. Coriell, R.F. Sekerka, J. Crystal Growth 34 (1976) 157.
[13] Y. Saito, Statistical Physics of Crystal Growth, World Scientific, Singapore, 1996.
[14] M.E. Glicksman, A. Lupulescu, M.B. Koss, J. Thermophys. Heat Transfer 17 (1) (2003) 69.
[15] M.E. Glicksman, R.J. Shaefer, J.D. Ayers, Metall. Trans. A 7A (1976) 1747.
[16] M.E. Glicksman, M.B. Koss, E.A. Winsa, Phys. Rev. Lett. 73 (1994) 573.
[17] J.C. LaCombe, M.B. Koss, M.E. Glicksman, Phys. Rev. Lett. 83 (1999) 2997.
[18] J. Alkemper, R. Mendoza, P.W. Voorhees, Adv. Eng. Mater. 4 (2002) 694.
[19] J. Alkemper, P.W. Voorhees, Acta Mater. 49 (2001) 897.
[20] A. Pimpinelli, J. Villain, Physics of Crystal Growth, Cambridge University Press, Cambridge, 1998.
[21] W.W. Mullins, R.F. Sekerka, J. Appl. Phys. 34 (2) (1963) 323.
[22] S.R. Coriell, R.L. Parker, J. Phys. 36 (1965) 632.
[23] S.R. Coriell, R.L. Parker, in: H.S. Peiser (Ed.), Crystal Growth, Pergamon Press, Oxford, 1967, p. 703.
[24] E. Ben-Jacob, P. Garik, Nature 343 (1990) 523.
[25] E. Ben Jacob, G. Deutscher, P. Garik, N.D. Goldenfeld, Y. Lareah, Phys. Rev. Lett. 57 (1986) 1903.
[26] H.S. Hele-Shaw, Nature 58 (1898) 34.
[27] J.V. Maher, Phys. Rev. Lett. 54 (1985) 1498.
[28] S. Osher, B. Merriman, Asian J. Math. 1 (1997) 560.
[29] G. Wulff, Z. Kristallogr. Mineral. 34 (1901) 449.
[30] F.S. Ham, Quart. Appl. Math. 17 (1959) 137.
[31] G. Horvay, J.W. Cahn, Acta Metall. 9 (1961) 695.
[32] S. Li, Morphological control of crystal growth, Ph.D. Thesis, University of Minnesota, 2005, (Expected).
[33] S.C. Hardy, S.R. Coriell, J. Res. Bureau of Standards–A Physics and Chemistry 73A (1) (1969) 65.
[34] J.Y. Zhu, X.F. Chen, T.Y. Hou, J. Comp. Phys. 127 (1996) 246.
[35] S.G. Mikhlin, Integral Equations and their Applications to Certain Problems in Mechanics, Mathematical Physics and Technology, Pergamon Press, New York, 1957.
[36] T.Y. Hou, J.S. Lowengrub, M.J. Shelley, J. Comp. Phys. 169 (2) (2001) 302.
[37] H.J. Jou, P. Leo, J. Lowengrub, J. Comp. Phys. 131 (1997) 109.
[38] S. Li, P. Leo, J. Lowengrub, V. Cristini, Nonlinear effect of surface tension anisotropy on the control of the Mullins–Sekerka instability, J. Appl. Phys. submitted.
[39] W.W. Mullins, R.F. Sekerka, J. Appl. Phys. 35 (2) (1964) 444.